Journal of Applied Mechanics and Technical Physics, Vol. 38, No. 3, 1997

GENERATION OF THREE-DIMENSIONAL BENDING VIBRATIONS OF A FLOATING ELASTIC PLATE IN MOTION OF A CONCENTRATED LOAD ALONG A COMPLEX TRAJECTORY

A. E. Bukatov and V. V. Zharkov

UDC 532.593:539.3:624.131

We study three-dimensional bending vibrations of a thin elastic plate which are excited by a concentrated load upon the motion of this plate in a circle whose center shifts rectilinearly with constant velocity. Analysis of the plate vibrations versus its bending rigidity, the angular velocity of loading, and the velocity of the center of its trajectory is given.

The structure of three-dimensional bending gravity waves excited by a constant and variable-intensity load moving rectilinearly over the surface of a floating plate has been studied in [1–5] and [6], respectively. Vibrations of a plate with a load moving in a circular trajectory have been studied in [7].

1. Let a thin elastic isotropic plate float over the surface of an ideal uniform incompressible liquid with a constant depth H. We shall consider three-dimensional bending vibrations of the plate excited by a concentrated load

$$p = p_0\delta(x - x_0)\delta(y - y_0), \quad x_0 = vt + r\cos(\omega t + \varphi_0), \quad y_0 = r\sin(\omega t + \varphi_0), \tag{1.1}$$

which moves with constant angular velocity ω in a circle of radius r whose center shifts rectilinearly with a constant velocity v. At zero moment ($t = 0$), the load is applied at the point $(r\cos\varphi_0, r\sin\varphi_0)$ of the circle.

Assuming the motion of a liquid to be potential and the wave velocities of its particles and the amplitudes of continuous vibrations of the plate to be small, we reduce the problem to the solution of the Laplace equation

$$\Delta\Phi = 0, \quad -H < z < 0, \quad -\infty < x, y < \infty \tag{1.2}$$

with the boundary conditions

$$D_1\nabla^4\zeta + æ_1\zeta_{tt} + \zeta + \Phi_t/g = -p_1, \quad \zeta_t = \Phi_z, \quad z = 0, \quad \Phi_z = 0, \quad z = -H \tag{1.3}$$

and the initial conditions

$$\Phi(x, y, z, 0) = \zeta(x, y, 0) = 0. \tag{1.4}$$

Here

$$\{D_1, æ_1, p_1\} = \{D, æ, p\}(\rho g)^{-1}; \quad D = \frac{Eh^3}{12(1-\nu^2)}; \quad \nabla^2 = \frac{\partial^2}{\partial x^2} + \frac{\partial^2}{\partial y^2}; \quad \Delta = \nabla^2 + \frac{\partial^2}{\partial z^2};$$

$\nabla^4 = (\nabla^2)^2$; $æ = \rho_1 h$; E, h, ρ_1, and ν are, respectively, the elasticity modulus, thickness, density, and Poisson's ratio of the plate, respectively; ρ is the liquid density, and Φ is the velocity potential of motion of a liquid particle.

To solve problem (1.1)–(1.4), we apply a complex Fourier transform in variables x and y and satisfying the boundary conditions in a coordinate system with the origin at the center of a circular trajectory, and we

Naval Hydrophysical Institute, Ukrainian Academy of Sciences, Sevastopol' 335000. Translated from Prikladnaya Mekhanika i Tekhnicheskaya Fizika, Vol. 38, No. 3, pp. 164–173, May–June, 1997. Original article submitted April 24, 1995; revision submitted January 19, 1996.

0021-8944/97/3803-0475 $18.00 © 1997 Plenum Publishing Corporation

obtain the equation

$$\left[\left(\frac{\partial}{\partial t} + ikv\cos\theta\right)^2 + \tau^2\right]\zeta^* = (2\pi)^{-1}\tau_0^2 p_1^* \exp(-irk\cos\alpha), \tag{1.5}$$

where $\tau_0^2 = (1 + æ_1 kg \tanh kH)^{-1} kg \tanh kH$, $\tau^2 = \tau_0^2 D_0(k)$, $D_0 = D_1 k^4 + 1$, $k^2 = k_x^2 + k_y^2$, $\alpha = \omega t + \varphi_0 - \theta$. $k_x = k\cos\theta$ and $k_y = k\sin\theta$ are the variables of the Fourier transform, and ζ^* and p_1^* are the Fourier transformants of ζ and p_1, respectively.

Using the known expansion of the function $\exp(-irk\cos\alpha)$ into a series of the Bessel functions [8] and satisfying the initial conditions written in polar coordinates, for plate bending (rise of the plate-liquid surface), we have the relation

$$\zeta = \frac{1}{4\pi^2}\int_{-\pi/2}^{3\pi/2}\int_0^\infty \sum_{n=0}^\infty B(k_x, k_y)(M_1 + M_2)\exp(i\lambda)\,dk\,d\theta. \tag{1.6}$$

Here

$$M_1 = S_1[\tau\cos(n\alpha) - N_1\exp(-ikvt\cos\theta)]; \qquad M_2 = iS_2[\tau\sin(n\alpha) + N_2\exp(-ikvt\cos\theta)];$$

$$N_1 = \tau\cos(\tau t)\cos(n\theta) + [ikv\cos\theta\cos(n\theta) + n\omega\sin(n\theta)]\sin(\tau t);$$

$$N_2 = \tau\cos(\tau t)\sin(n\theta) + [ikv\cos\theta\sin(n\theta) - n\omega\cos(n\theta)]\sin(\tau t);$$

$$S_1 = \tau^2 - (kv\cos\theta)^2 - (n\omega)^2; \qquad S_2 = 2n\omega kv\cos\theta;$$

$$B = i^n[D_0(S_1^2 - S_2^2)]^{-1}(2 - \delta_{n,0})J_n(kr)k\tau p_1^*; \quad \lambda = kR\cos(\theta - \gamma); \quad R = (x^2 + y^2)^{1/2};$$

$x = R\cos\gamma$, $y = R\sin\gamma$, and $\delta_{n,0}$ is the Kronecker symbol.

On the path of integration over θ, there can be singularities at the points $\theta = \theta_{ln}$ ($l = 1,2,\ldots,8$), where $\theta_{1n} = \arccos\tau_{1n}$; $\theta_{2n} = -\theta_{1n}$; $\theta_{3n} = \pi - \theta_{1n}$; $\theta_{4n} = \pi + \theta_{1n}$; $\theta_{5n} = \arccos\tau_{2n}$; $\theta_{6n} = -\theta_{5n}$; $\theta_{7n} = \pi - \theta_{5n}$; $\theta_{8n} = \pi + \theta_{5n}$; $\tau_{sn} = (kv)^{-1}[\tau + (-1)^s n\omega]$ ($s = 1$ and 2).

The poles θ_{ln} ($l = 1,\ldots,4$) lie in the interval $[-\pi/2, 3\pi/2]$ of the real θ axis if $\tau_{1n}^2 \leqslant 1$. Under this condition, the wave number k varies in the interval (k_1, k_2) if one of the inequalities

$$n\omega \geqslant \sigma_0, \quad v \leqslant v_{01}, \quad v \geqslant v_{02} \tag{1.7}$$

is satisfied. If

$$n\omega < \sigma_0, \quad v_{01} < v < v_{02}, \tag{1.8}$$

to the condition $\tau_{1n}^2 \leqslant 1$ correspond two intervals of variation in the wave number: (k_1, k_1^*) and (k_2^*, k_2).

The real poles θ_{ln} ($l = 5,\ldots,8$) exist on the θ axis for such $\tau_{2n}^2 \leqslant 1$ if

$$v \geqslant v_{03}. \tag{1.9}$$

With satisfaction of (1.9), the wave number k varies in the (k_3, k_4) interval. In the case where $v < v_{03}$, the poles on the real axis θ are absent for any real k, because $\tau_{2n}^2 > 1$. If $n = 0$, for $\tau_{2n}^2 \leqslant 1$, and $v > c$, then $k_3 = 0$. Here $\sigma_0 = [\beta_2\tau(\beta_1) - \beta_1\tau(\beta_2)](\beta_2 - \beta_1)^{-1}$, $v_{01} = v\tau_{1n}(\beta_2)$, $c = (gH)^{1/2}$, $v_{02} = v\tau_{1n}(\beta_1)$, $v_{03} = v\tau_{2n}(\beta_3)$, $\tau_{1n}^*(\beta_1) = \tau_{1n}^*(\beta_2) = \tau_{2n}^*(\beta_3) = 0$, $\tau_{sn}^* = \tau_{sn} - \tau_1$ ($s = 1, 2$), $\tau_1 = (1/v)\partial\tau/\partial k$; k_1, k_1^*, k_2^*, and k_2 are the positive roots of the equation $\tau_{1n} = 1$, and k_3 (if $n \neq 0$ or $n = 0, v \leqslant c$) and k_4 are the roots of the equation $\tau_{2n} = 1$.

Let us choose the bypasses of the poles θ_{ln} in the complex plane in such a way that the inequality $\mathrm{Re}(-ivkt\cos\theta) < 0$ is fulfilled. This ensures the damping of N_1 and N_2 and the appearance of a periodic-in-time wave picture that is characterized by integral (1.6). Since v, k, and t are positive, we shall bypass θ_{ln} for an odd, from above, and even, from below, value of l. The integration contours obtained are denoted by L_{mn},

and Eq. (1.6) is written in the form

$$\zeta = (8\pi^2)^{-1} \sum_{m=1}^{2} \sum_{n=0}^{\infty} (I_{1mn} - I_{2mn}) + O(R^{-1}),$$

$$I_{1mn} = \int_{L_{mn}} \int_{L^*_{mn}} B_{mn}(k,\theta)\tau \exp\left[i(\lambda - (-1)^m n\alpha)\right] dk\, d\theta,$$

$$I_{2mn} = \int_{L_{mn}} \int_{L^*_{mn}} B_{mn}(k,\theta) N^* \exp[i(\lambda - kvt\cos\theta - (-1)^m n\alpha)] dk d\theta, \tag{1.10}$$

$$N^* = \tau\cos(\tau t) + i[kv\cos\theta + (-1)^m n\omega]\sin(\tau t),$$

$$B_{mn} = i^n(2 - \delta_{n,0}) D_0^{-1}[S_1 - (-1)^m S_2]^{-1} J_n(kr) k\tau p_1^*,$$

where the contours L_{1n} bypass the poles θ_{ln} ($l = 3$, 4, 5, and 6), while L_{2n} bypasses the poles θ_{ln} ($l = 1$, 2, 7. and 8). The integration over the wave number is performed along the intervals L^*_{mn} of the real k axis which are the domains of definition of the poles θ_{ln} upon satisfaction of conditions (1.7)–(1.9).

We shall supplement the contours L_{mn} to make them closed with allowance for the conditions

$$\mathrm{Re}\,[i(\lambda - (-1)^m n\theta)] \leqslant 0, \quad \mathrm{Re}\,[i(\lambda - kvt\cos\theta - (-1)^m n\theta)] \leqslant 0,$$

that ensure the boundedness of the intervals I_{1mn} and I_{2mn} at $R \to \infty$. For fixed m and n, each of the closed contours obtained contains the same poles if $\mathrm{sign}[kR\sin(\theta - \gamma) + (-1)^m n] = \mathrm{sign}[kR\sin(\theta - \gamma) + (-1)^m n - kvt\sin\theta]$.

This equality is satisfied if $R > R_{mn} + Ut$ or $R < R_{mn} - Ut$, where $R_{mn} = (-1)^{m+1} n/[k\sin(\theta - \gamma)]$ and $U = v|\sin\theta/\sin(\theta - \gamma)|$. Under these conditions, I_{1mn} and I_{2mn} compensate for each other with accuracy up to perturbation damping with distance as $O(R^{-1})$. The residues in the corresponding poles θ_{ln} represent the periodic wave motion in the regions $0 \leqslant R \leqslant R_{mn} + Ut$ if $t \geqslant t_n = n/(kv|\sin\theta|)$ and in the regions $R_{mn} - Ut \leqslant R \leqslant R_{mn} + Ut$ if $R_{mn} \geqslant 0$ and $t < t_n$. Thus, the quantity $U = U_{ln}$ is the velocity of the leading front of perturbations characterized by the pole $\theta = \theta_{ln}$.

Applying the residue theorem, from (10) we obtain

$$\zeta = K_{20} + \sum_{n=1}^{\infty} (K_{1n} + K_{2n}) + O(R^{-1}), \tag{1.11}$$

where, for fixed n, the expression for K_{1n} has the form

$$K_{1n} = \sum_{l=1}^{4} \int_{k_1}^{k_2} G^*_{ln}(k)\, dk, \quad K_{1n} = \sum_{l=1}^{4} \left(\int_{k_1}^{k_1^*} G^*_{ln}(k)\, dk + \int_{k_2^*}^{k_2} G^*_{ln}(k)\, dk \right)$$

provided that conditions (1.7) and (1.8), respectively, are satisfied. If $v < v_{03}$, then $K_{2n} = 0$, and under condition (1.9)

$$K_{2n} = \sum_{l=5}^{8} \int_{k_3}^{k_4} G^*_{ln}(k)\, dk.$$

Here

$$G^*_{ln}(k) = \begin{cases} G_{ln}(k), & \theta_{1n}(k) - \pi + \chi_n(k) < \gamma < \theta_{1n}(k) - \chi_n(k), \\ 0, & \theta_{1n}(k) - \chi_n(k) \leqslant \gamma \leqslant \theta_{1n}(k) + \pi + \chi_n(k) \end{cases} \quad \text{for} \quad l = 1,\ 4;$$

$$G^*_{ln}(k) = \begin{cases} G_{ln}(k), & -\theta_{1n}(k) - \chi_n(k) < \gamma < \pi - \theta_{1n}(k) + \chi_n(k), \\ 0, & \pi - \theta_{1n}(k) + \chi_n(k) \leqslant \gamma \leqslant 2\pi - \theta_{1n}(k) - \chi_n(k) \end{cases} \quad \text{for} \quad l = 2,\ 3;$$

TABLE 1

l	j	m	s	l	j	m	s
1	1	2	1	5	1	1	2
2	2	2	1	6	2	1	2
3	2	1	1	7	2	2	2
4	1	1	1	8	1	2	2

$$G^*_{ln}(k) = \begin{cases} G_{ln}(k), & \theta_{5n}(k) - \pi - \chi_n(k) < \gamma < \theta_{5n}(k) + \chi_n(k), \\ 0, & \theta_{5n}(k) + \chi_n(k) \leqslant \gamma \leqslant \theta_{5n}(k) + \pi - \chi_n(k) \quad \text{for} \quad l = 5, 8; \end{cases}$$

$$G^*_{ln}(k) = \begin{cases} G_{ln}(k), & -\theta_{5n}(k) + \chi_n(k) < \gamma < \pi - \theta_{5n}(k) - \chi_n(k), \\ 0, & \pi - \theta_{5n}(k) - \chi_n(k) \leqslant \gamma \leqslant 2\pi - \theta_{5n}(k) + \chi_n(k) \quad \text{for} \quad l = 6, 7; \end{cases}$$

$$\chi_n(k) = \begin{cases} \arcsin(n/(kR)), & k > n/R, \\ \pi/2, & k \leqslant n/R; \end{cases} \qquad G_{ln}(k) = (8\pi^2)^{-1}\Psi_{ln}(k)J_n(kr)\exp[i\psi_{ln}(k)];$$

$\psi_{ln}(k) = kR\cos(\theta_{ln} - \gamma) + (-1)^m n[\omega t + \varphi_0 + (-1)^j\theta_{bn}] + n_0\pi/2$; $\Psi_{ln}(k) = (2 - \delta_{n,0})(D_0\sigma^*_{sn}v)^{-1}\tau p^*_1$; $\sigma^*_{sn} = (1 - \tau^2_{sn})^{1/2}$; $n_0 = n + [(-1)^n + 1](s - m + 1) + 1$; and $b = 4s - 3$ for $l = 1, 2, \ldots, 8$.

To the value l of the pole θ_{ln} correspond j, m, and s from Table 1.

Using the asymptotic representation $J_n(kr) \approx (2/\pi kr)^{1/2}\cos(kr - n\pi/2 - \pi/4)$, we write the expression for G_{ln} in the form

$$G_{ln}(k) = \frac{1}{8\pi^2\sqrt{2\pi kr}}\Psi_{ln}(k)\sum_{q=1}^{2}\exp\left[i\left(\psi_{ln}(k) + (-1)^q\left(rk - n\frac{\pi}{2} - \frac{\pi}{4}\right)\right)\right]$$

and analyze integrals (1.11) by the stationary-phase method. As a result, for the amplitude of perturbations along the constant-phase curve, we obtain the expression

$$A(k) = \frac{(2 - \delta_{n,0})\tau p^*_1}{8\pi^2 v D_0}\left[\frac{k\tau^*_{sn}\sigma^*_{sn}}{r|Z(k)|}\right]^{1/2}, \tag{1.12}$$

and write the equation for the constant-phase curve as

$$x(k) = [(1 - \tau_{sn}\tau_1)\mu + \sigma^*_{sn}\eta](k\tau^*_{sn})^{-1}, \quad y(k) = (-1)^j(\tau_1\sigma^*_{sn}\mu + \tau_{sn}\eta)(k\tau^*_{sn})^{-1}. \tag{1.13}$$

Here

$$\mu = (-1)^s n\varphi_1 - (-1)^q kr + \pi\varphi_2; \quad \eta = (-1)^q kr\sigma^*_{sn} - (-1)^s n\tau^*_{sn};$$

$$\varphi_1 = \omega t + \varphi_0 + (-1)^j \arccos\tau_{sn}; \quad \varphi_2 = 2(N - n^*) + \xi_0 + [(-1)^q(n + 1/2) + n_0]/2;$$

$$Z(k) = \mu\sigma^*_{sn}Z_1(k) + \eta Z_2(k) - (-1)^s n\tau^*_{sn}Z_3(k); \quad Z_1(k) = \tau_2(\sigma^*_{sn})^2 + \tau_1(\tau^*_{sn})^2;$$

$$Z_2(k) = \tau_2(\sigma^*_{sn})^2 + \tau_{sn}(\tau^*_{sn})^2; \quad Z_3(k) = [\tau_{sn}(\tau_{sn} + \tau_1) - 2]\tau^*_{sn} - \tau_2(\sigma^*_{sn})^2; \quad \tau_2 = \frac{k}{v}\frac{\partial^2\tau}{\partial k^2};$$

k varies on the intervals of definition of the poles θ_{ln} which correspond to conditions (1.7)–(1.9) and to which s and j from Table 1 correspond; N is the number of the curve considered from the coordinate origin, $\pi\xi_0$ is its phase shift determined by the sign of $Z(k)$, n^* is an integer of $n/4$, and q takes on the values 1 or 2.

2. An analysis of the solution obtained has shown that the structure and character of the excited periodic wave motion is mainly determined by the bending rigidity of the plate and also by the angular and translational velocities of load displacement.

For each fixed mode with number n, there exist seven critical values of the velocity of translational motion of the load (v_{01}, v_{02}, v_{03}, v_{10}, v_{11}, v_{12}, c) and one critical angular frequency σ_0, in passing through which the character and structure of the periodic perturbations change. Among them, the quantities σ_0, v_{01},

v_{02}, v_{03}, and c are the same as in (1.7)–(1.9), and, for v_{10}, v_{11}, and v_{12}, the formulas

$$v_{11} = v[\tau_3(\beta_4)]^{1/2}, \quad v_{12} = v[\tau_4(\beta_6)]^{1/2}, \quad v_{10} = v[\tau_5(\beta_8)]^{1/2}, \quad \tau_3 = \tau_{1n}^2 - (\tau_{1n} - \tau_1)^2\tau_1/\tau_2,$$

$$\tau_4 = \tau_{2n}^2 - (\tau_{2n} - \tau_1)^2\tau_1/\tau_2, \quad \tau_5 = \tau_{1n}\tau_1, \quad \tau_6 = (\tau_1)^2 - \tau_{1n}(\tau_1 - \tau_2), \quad \tau_6(\beta_8) = \tau_6(\beta_9) = 0,$$

$$\Theta_1''(\beta_4) = \Theta_1''(\beta_5) = \Theta_2''(\beta_6) = \Theta_2''(\beta_7) = 0, \quad \Theta_s(k) = \tau_1\sigma_{sn}^*(1 - \tau_{sn}\tau_1)^{-1} \quad (s = 1, 2),$$

$$\beta_4 < \beta_5, \quad \beta_6 < \beta_7, \quad \beta_8 < \beta_9$$

are valid (the primes denote the derivatives with respect to k).

Depending on the generation conditions, from one to seven ($i^* = 1, \ldots, 7$) pairs ($q = 1$ and 2) of wave systems can be excited; $i^* = 1$ and 5 corresponds to the transverse gravity and $i^* = 2$ and 6 to the longitudinal gravity waves of the ship-borne type. The waves with $i^* = 3$ and 7 are bending and are due to the plate rigidity, while $i^* = 4$ corresponds to the system of a helix-shaped form which are due to the angular velocity of pressure displacement. In (1.13), $i^* = 1, \ldots, 4$ corresponds to $s = 1$, and $i^* = 5, \ldots, 7$ corresponds to $s = 2$. For the crests of transverse gravity, bending, and helix-shaped waves, $\xi_0 = -3/4$, and, for those of longitudinal gravity waves, $\xi_0 = -1/4$.

In the wave pattern, to the boundaries of the angular zones of the wave systems correspond the caustics along which the amplitudes drop according to the law $R^{-1/3}$. They can be found using the break points of the constant-phase curves which occur at $Z(k) = 0$ and correspond to a transition to a new system. With distance from the load, in the region $R \geqslant r$ the opening angles of the zones of wave perturbations which are due to the subsystems $q = 1$ and 2 of each pair i^* approach asymptotically the quantities $\gamma_2 = \arctan\Theta_1(\alpha_2)$, $\gamma_{11} = \arctan\Theta_2(\alpha_3)$, $\gamma_{22} = \arctan\Theta_2(\alpha_4)$, $\gamma_1 = \arctan\Theta_1(\alpha_1)$ for $v_{11} < v < v_{02}$, $\gamma_3 = \arctan\Theta_1(\alpha_1)$ for $v > v_{02}$, and $\gamma_{12} = \arctan\Theta_2(0)$ for $n\omega = 0$ and $v > c$; $\Theta_1'(\alpha_1) = \Theta_1'(\alpha_2) = \Theta_2'(\alpha_3) = \Theta_2'(\alpha_4) = 0$, where $\alpha_1 < \alpha_2$, $\alpha_3 < \alpha_4$.

Their correspondence to the number of i^* is shown in Tables 2 ($s = 1$) and 3 ($s = 2$) that characterize the phase structure of wave perturbations in the region $R \geqslant r$.

The quantities γ_1, γ_2, γ_3, γ_{11}, and γ_{22} that characterize the angular zones of the steady perturbations which are due to the n mode and the displacement velocities v_{01}, v_{02}, v_{03}, v_{10}, v_{11}, and v_{12} of the load depend on $n\omega$ in the same way as on the pulsation frequency σ of a translationally moving source of variable intensity. This dependence was studied by Bukatov and Yaroshenko in [6]. In addition, for $\sigma = n\omega$, the dependence of the indicated quantities on the characteristics of the plate was considered.

3. The phase structure of perturbations which are due to each pair of excited wave subsystems of the first and second modes was analyzed on the basis of expressions (1.13) for $E = 3 \cdot 10^9$ N$\cdot$m^{-2}, $\nu = 0.34$, and $\rho_1 = 0.87 \cdot 10^3$ kg$\cdot$m^{-3} that characterize an icy plate [9, 10]. Here the depth of a reservoir is 10^3 m, the thickness of the ice cover is 2 m, and the water density is 10^3 kg$\cdot$m^{-3}. The radius of the trajectory of load displacement is $r = 10^2$–10^3 m, its translational velocity is $v = 10^{-1}$–40 m$\cdot$sec^{-1}, and the angular velocity $\omega = 5 \cdot 10^{-2}$–10^{-1} sec^{-1} for $\varphi_0 = 0$ at different stages of the oscillation period. The translational motion of the load occurs in the negative direction of the x axis, and its rotary motion occurs clockwise.

An analysis has shown that, for the v values satisfying the inequalities $v_{01} < v < v_{02}$ and $n\omega < \sigma_0$ or $v_{11} < v < c$ and $n\omega > 0$, the structure of the generated wave perturbation is a superposition of seven wave subsystems.

Their wave patterns are illustrated in Figs. 1–3 for $v = 40$ m$\cdot$sec^{-1}, $\omega = 5 \cdot 10^{-2}$ sec^{-1}, $r = 3 \cdot 10^2$ m, and the phase of load rotation π. These figures show the constant-phase (crests) curves of the helix-shaped [$i^* = 4$ (Fig. 1)], transverse gravity, longitudinal ship-borne, and bending waves [$i^* = 1, \ldots, 3$ (Fig. 2) and $i^* = 5, \ldots, 7$ (Fig. 3)] of the first mode. The thick and thin curves refer to $q = 1$ and 2, respectively. The solid curves in Figs. 2 and 3 show bending waves, and the dot-and-dashed curves with one and two dots show longitudinal and transverse gravity ones of the ship-borne type. The bounds of the angular zones of the corresponding subsystems are shown by dashed curves. The dotted curve in Figs. 2 and 3 shows the trajectory of circular pressure displacements in the coordinate system connected to its center. The circle at the center of Fig. 1 also refers to this trajectory.

It is seen that the crests of helix-shaped waves originate at points half a wavelength away from the

TABLE 2

v	$\gamma(\pm 2\pi)$	i^*	$n\omega$
$0 < v < v_{01}$	$0 \leqslant \gamma \leqslant 2\pi$	4	$0 < n\omega < \sigma_0$
$v_{01} < v < v_{11}$	$0 \leqslant \gamma \leqslant 2\pi$	3, 4	
$v_{11} < v < v_{02}$	$-\gamma_2 < \gamma < \gamma_2$	1, 4	
	$-\gamma_1 \leqslant \gamma \leqslant -\gamma_2$, $\gamma_2 \leqslant \gamma \leqslant \gamma_1$	1, 2, 3,4	
	$\gamma_1 < \gamma < 2\pi - \gamma_1$	3, 4	
$v_{02} < v < v_{10}$	$-\gamma_2 < \gamma < \gamma_2$	4	
	$-\gamma_3 \leqslant \gamma \leqslant -\gamma_2$, $\gamma_2 \leqslant \gamma \leqslant \gamma_3$	2, 3, 4	
	$\gamma_3 < \gamma < 2\pi - \gamma_3$	3	
$v > v_{10}$	$-\gamma_2 < \gamma < \gamma_2$	1	
	$-\gamma_1 \leqslant \gamma \leqslant -\gamma_2$, $\gamma_2 \leqslant \gamma \leqslant \gamma_1$	1, 2, 3	
	$\gamma_1 < \gamma < 2\pi - \gamma_1$	3	
$0 < v < v_{11}$	$0 \leqslant \gamma \leqslant 2\pi$	4	$n\omega > \sigma_0$
$v > v_{11}$	$-\gamma_2 \leqslant \gamma \leqslant \gamma_2$	4	
	$-\gamma_3 \leqslant \gamma \leqslant -\gamma_2$, $\gamma_2 \leqslant \gamma \leqslant \gamma_3$	2, 3, 4	
	$\gamma_3 < \gamma < 2\pi - \gamma_3$	3	

TABLE 3

v	$\gamma(\pm 2\pi)$	i^*	$n\omega$
$v < v_{03}$	$0 \leqslant \gamma \leqslant 2\pi$	—	$n\omega \geqslant 0$
$v_{03} < v < v_{12}$	$0 \leqslant \gamma \leqslant 2\pi$	7	
$v_{12} < v < c$	$-\gamma_{22} < \gamma < \gamma_{22}$	5	
	$-\gamma_{11} \leqslant \gamma \leqslant -\gamma_{22}$, $\gamma_{22} \leqslant \gamma \leqslant \gamma_{11}$	5, 6, 7	
	$\gamma_{11} < \gamma < 2\pi - \gamma_{11}$	7	
$v > c$	$-\gamma_{22} \leqslant \gamma \leqslant \gamma_{22}$	5	$n\omega > 0$
	$-\gamma_{11} \leqslant \gamma \leqslant -\gamma_{22}$, $\gamma_{22} \leqslant \gamma \leqslant \gamma_{11}$	5, 6, 7	
	$\gamma_{11} < \gamma < 2\pi - \gamma_{11}$	7	
	$-\gamma_{12} \leqslant \gamma \leqslant \gamma_{12}$	—	$n\omega = 0$
	$-\gamma_{11} \leqslant \gamma \leqslant -\gamma_{12}$, $\gamma_{12} \leqslant \gamma \leqslant \gamma_{11}$	6, 7	
	$\gamma_{11} < \gamma < 2\pi - \gamma_{11}$	7	

pressure-displacement trajectory. The crest number increases with each turn of the helix. The wavelengths are approximately equal for both subsystems. Note that they are minimal on the abscissa before the load and maximal behind it. The minimal wavelength exceeds substantially the radius of the circular trajectory of load motion. In addition, the lengths of helical waves depend weakly on this radius. The difference in the wavelengths in front of or behind the loads is determined by the translational velocity of its motion. The difference decreases as the velocity drops to zero. The system of helical perturbations is generated at any value of the velocity within the interval $0 \leqslant v < v_{10}$ if $n\omega < \sigma_0$ and within the interval $v \geqslant 0$ if $n\omega < \sigma_0$.

Note that gravity waves of the helical type are excited in a free-surface fluid under the motion of a perturbation source in a circular trajectory [11, 12].

The systems of bending, longitudinal, and transverse gravity waves of each of two subsystems form two superimposing patterns, which are similar to the known ones from [1, 2, 4] for a translationally moving generator of constant intensity. This is true for $s = 1$ and 2 (Figs. 2 and 3). The ranges of wavelength variation of either subsystems are equal. The bending waves have a minimal length, and the transverse gravity ones have a maximal one. The angular zones (where perturbations are generated) which are due to the joint contribution of the systems of bending, longitudinal, and transverse gravity waves are considerably smaller at $s = 2$ than at $s = 1$.

Unlike the case of a translationally moving load, asymmetry of the phase patterns relative to the line of displacement of the center of its trajectory is observed. This is especially noticeable in the shapes of the crest of gravity transverse waves and also in the position of the vertices of the angular three-wave perturbation zones.

For subsystems with $q = 1$ (thin curves), the bending waves-precursors border the circular trajectory before loading. The angular three-wave perturbation zones behind the load intersect, passing through the abscissa axis. The first crests of gravity transverse waves are formed only behind the region of intersection of

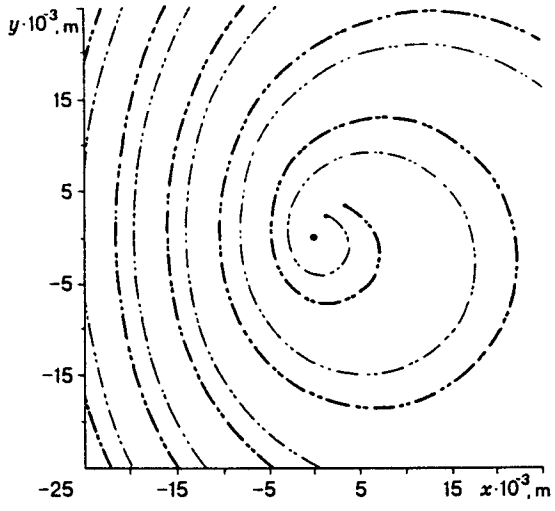

Fig. 1

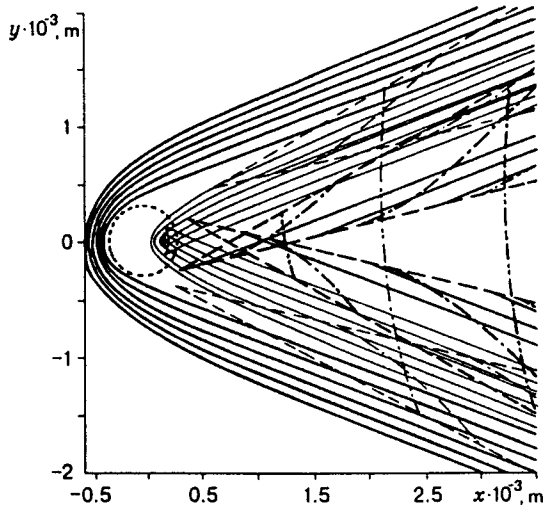

Fig. 2

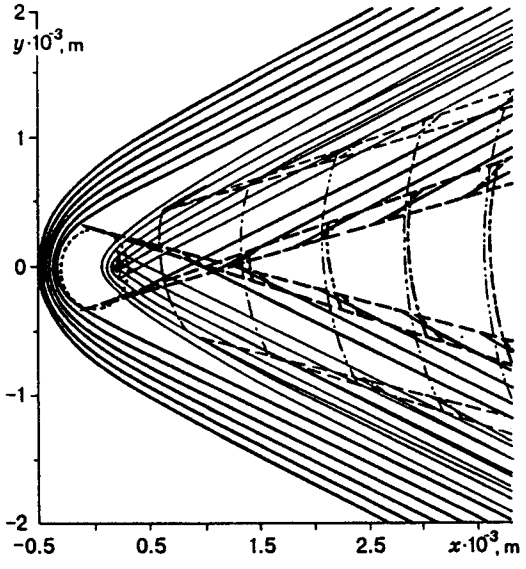

Fig. 3

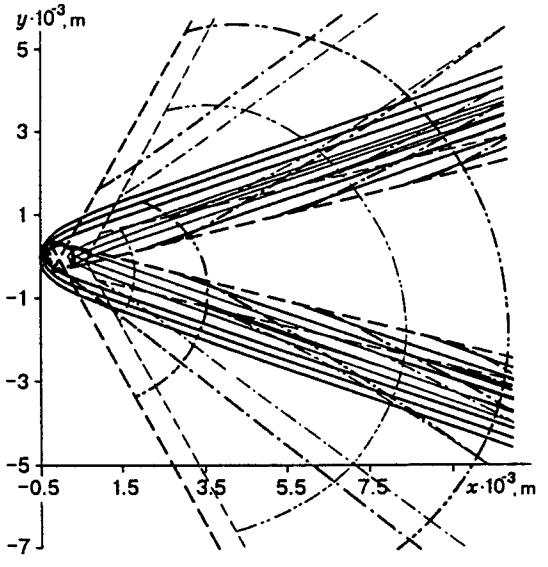

Fig. 4

the angular zones. For subsystems with $q = 2$ (thick curves), the crests of the bending waves can either enter the trajectory-bounded region or be positioned in front of this region. In this case, the first constant-phase curves inside this region can break and intersect the x axis behind it. The angular three-wave perturbation zones do not cross each other. Their vertices are far from the load, and the opening angles in the zone considered are smaller than those for $q = 1$. In this case, the zone of generation of transverse ship waves is considerably wider as compared with the $q = 1$ case.

Note that the number of broken crests of bending waves increases with increasing r. For fairly large r, the first crests of the transverse gravity waves can also be broken. A change of ωt gives rise to phase shifts in each wave subsystems considered.

The first crest of a gravity transverse wave from the subsystem with $q = 2$ becomes the crest of a bending one, bypassing the vertices of three-wave perturbation generation zones (Fig. 3). Such zones narrow, and their vertices become more distant as the velocity v diminishes to the critical v_{11} ($s = 1$, Fig. 2) or v_{12} ($s = 2$, Fig. 3). The number of crests of transverse gravity waves which become crests of bending waves increases as well. All wave crests behind the load in the velocity range $v_{01} < v < v_{11}$ ($s = 1$) or $v_{03} < v < v_{12}$ ($s = 2$) have a qualitatively similar shape. For such values of v, there are no three-wave

TABLE 4

Variant	i^*	q	γ, deg		
			20	40	120
			$A(k) \cdot 10/p_1$ (Λ, m)		
I	1	1	0.99 (1890)	—	—
		2	1.02 (1850)	—	—
	2	1	3.27 (704)	—	—
		2	3.53 (354)	—	—
	3	1	—	1.57$_-$ (78.7)	0.43$_-$ (39.0)
		2	3.18$_+$ (129)		
			2.13$_-$ (101)	1.30$_-$ (71.9)	0.40$_-$ (38.5)
	4	1	0.10 (14710)	0.13 (11430)	0.14 (7500)
		2	0.01 (17480)	0.01 (17310)	0.16 (7930)
	7	1	1.76$_+$ (103)	1.52$_-$ (78.9)	0.44$_-$ (39.4)
		2	3.16$_+$ (128)		
			2.53$_-$ (95.8)	1.31$_-$ (72.0)	0.41$_-$ (38.8)
II	2	1	2.06 (670)	1.53 (1510)	—
		2	3.46 (340)	—	—
	3	1	—	1.51$_-$ (78.2)	0.41$_-$ (38.8)
		2	2.26$_-$ (100)	1.30$_-$ (71.3)	0.39$_-$ (38.3)
	4	1	0.40 (7180)	0.43 (5860)	—
		2	0.05 (8270)	0.07 (7700)	—
	7	1	1.95$_+$ (101)	1.55$_-$ (79.1)	0.44$_-$ (39.6)
		2	3.12$_+$ (127)	1.36$_-$ (72.2)	0.42$_-$ (39.1)

perturbation zones. As the velocities increase to v_{01} ($s = 1$) or v_{03} ($s = 2$), the wave crests straighten in the direction perpendicular to the curve. For $v < v_{01}$ or $v < v_{03}$, the bending and gravity waves corresponding to $s = 1$ or $s = 2$ do not contribute to perturbation formation.

If $v_{02} < v < v_{10}$ and $n\omega < \sigma_0$ or $v > v_{11}$ and $n\omega > \sigma_0$, there is no contribution from ship-type transverse gravity waves to the formation of perturbations corresponding to $s = 1$. Only bending waves can be excited before loading in this case. In the wave wake, angular zones are formed in which the perturbation structure is formed by helix-shaped waves either along with longitudinal and bending waves or without them.

Figure 4 shows the phase picture under the conditions considered for the values of the parameters which correspond to Figs. 1–3 for $\omega = 10^{-1}$ sec^{-1}. The crests of the helix-shaped waves are shown by the dot-and-dashed curves with two points. The crests of the bending (solid curves) and transverse gravity (dot-and-dashed curves with one point) waves are shown through one crest. Evidently, the angular zones of three-wave perturbation generation for both subsystems ($q = 1$ and 2) are larger than those for the other velocity ranges considered. The curves of the first crests of helix-shaped waves cannot reach one of the bounds of the corresponding angular zone. The characteristic features of the subsystems with $q = 1$ and 2 are qualitatively the same as for the conditions of Figs. 2 and 3.

If $v > v_{10}$, and $n\omega < \sigma_0$, helix-type waves are not excited, and the phase pattern for $s = 1$ is similar to that shown in Fig. 2.

In the velocity ranges considered, the phase structure of the perturbations corresponding to $s = 2$ is qualitatively the same as that for the v values from other ranges (see Table 2) which correspond to $s = 1$.

The phase patterns of perturbations which are due to the first mode with frequency $n\omega$ are similar to those formed by the mode with number n with frequency ω.

4. A quantitative comparison of the possible contributions of the generated waves to the bending oscillations of the plate was performed using formulas (1.12) and (1.13) for the values of the starting parameters corresponding to the conditions of Figs. 1–3 (variant I) and Fig. 4 (variant II). In Table 4, the amplitudes $A(k)$ of bending that is due to each of the wave systems q of the systems i^* are given with accuracy up to the factor $10/p_1$ for three fixed points of the plane on the right from the path of motion of the load-trajectory center. These points are 5 km away from the origin of coordinates along the rays which constitute the angles $\gamma = 20$, 40, and 120°, respectively, with the x axis. The plus sign refers to the amplitudes of the subsystems of bending waves ($i^* = 3$ and 7) with $q = 1$ and 2 for which the constant-phase curves begin at the bound of the corresponding angular wave-wake zone, and the minus sign refers to bending waves with constant-phase curves which either border (in a moving coordinate system) the circular trajectory of load displacement (for $q = 1$ and 2) or enter inside the circle limited by this trajectory (for $q = 2$) (the local values of the lengths of the corresponding waves $\Lambda = 2\pi/k$ are given in brackets). A line indicates the absence of an appropriate wave system at the point under consideration. In addition, we note that there are waves corresponding to $i^* = 5$, 6 for variants I and II and to $i^* = 1$ for variant II at these points.

From the data in Table 4, it is clear that the plate-oscillation amplitudes due to bending and ship gravity waves are comparable, at the chosen points, with each other in order of magnitude despite the appreciable differences in the local values of these wavelengths. Here the effect of the helical waves on bending of the plate is less significant. However, the phase pattern of oscillations deforms as the generation conditions vary, and, hence, the contributions of the excited waves to plate bending at a fixed point redistribute. We should recall that, for $v < \min(v_{01}, v_{03})$, oscillations are formed only by helical waves.

This work was partially supported by the Joint Foundation of the Ukrainian Government and International Science Foundation (Grant No. K31 100).

REFERENCES

1. A. E. Bukatov and A. A. Yaroshenko, "Effect of a uniformly compressed floating plate on the development of three-dimensional waves in a homogeneous fluid," *Izv. Akad. Nauk SSSR, Mekh. Zhidk. Gaza*, No. 6, 78–83 (1984).
2. J. W. Davis, R. J. Hosking, and A. D. Sneyd, "Waves due to a steadily moving source on a floating ice plate," *J. Fluid Mech.*, **158**, 269–287 (1985).
3. V. A. Squaire, W. H. Robinson, T. G. Haskell, and S. G. Moore, "Dynamic strain response of lake and sea ice to moving loads," *Cold Reg. Sci. Tech.*, **11**, No. 2, 123–139 (1986).
4. R. M. S. M. Schulkes, R. J. Hosking, and A. D. Sneyd, "Waves due to a steadily moving source on a floating ice plate. Part II," *J. Fluid Mech.*, **180**, 297–318 (1987).
5. T. Takizawa, "Response of a floating sea ice sheet to a steadily moving load," *J. Geophys. Res.*, **93**, No. C5, 5100–5112 (1988).
6. A. E. Bukatov and A. A. Yaroshenko, "Development of three-dimensional bending gravity waves upon motion of a variable-intensity pressure region," *Zh. Prikl. Mekh. Tekh. Fiz.*, No. 5, 54–60 (1986).
7. A. E. Bukatov, "Bending gravity waves upon motion of pressures along a circular trajectory," in: *Theoretical and Experimental Studies of Wave Processes in an Ocean* (Collected scientific papers) [in Russian], Naval Hydrophys. Inst., Ukrainian Acad. of Sci. (1991), pp. 37–41.
8. B. G. Korenev, *Introduction to the Theory of Bessel Functions* [in Russian], Moscow, Nauka (1971).
9. D. E. Kheisin, *Dynamics of Ice Cover* [in Russian], Gidrometeoizdat, Leningrad (1967).
10. V. V. Bogorodskii and V. P. Gavrilo, *Ice. Physical Properties. Modern Methods of Glaciology* [in Russian], Gidrometeoizdat, Leningrad (1980).
11. S. V. Alekseenko and A. A. Cherep, "Formation of helical waves upon circular motion of a source in a dispersing medium," *Dokl. Ross. Akad. Nauk*, **327**, No. 3, 306–310 (1992).